In-ring nuclear reaction induced by light-ions at HIRFL-CSR*

Guo Qiang Zhang (张国强)[1,2] Liu Yuan Li (李柳圆)[2,3] Xiao Lin Tu (涂小林)[2†] Yu Huang (黄宇)[2] Jing Tao Zhang (张景涛)[2] Qi Gao (高启)[1‡] and CSRe cooperation group

[1]The Key Laboratory of Cosmic Rays (Xizang University), Ministry of Education, Lhasa 850000, China
[2]Institute of Modern Physics, Chinese Academy of Sciences, Lanzhou 730000, China
[3]School of Nuclear Science and Technology, Lanzhou University, Lanzhou 730000, China

Abstract: In-ring nuclear reactions induced by light-ions, which are characterized by low-momentum sensitivity and low background, play an important role in nuclear structure and astrophysics investigations. Recently, the in-ring proton-nucleus elastic scattering measurements at low momentum transfer based on the internal hydrogen-gas-jet target have been successfully performed at the Cooler Storage Ring of the Heavy Ion Research Facility in Lanzhou (HIRFL-CSR). In this proceeding, we present the progress of matter radius measurements using the small-angle differential cross sections of proton-nucleus elastic scattering at HIRFL-CSR.

Keywords: elastic scattering, inverse kinematics, cooler storage ring, gas-jet target

DOI: 10.1088/1674-1137/adc122 **CSTR:** 32044.14.ChinesePhysicsC.49074002

I. INTRODUCTION

Nuclear size measurements have a long history since the Geiger-Marsden alpha scattering experiment in 1908 [1]. Based on the experiment, atomic nucleus with a small size of $\sim 10^{-15}$ m was discovered. Consequently, the Rutherford atomic model was established in 1911 [2]. Since then, the open issue of how the nucleus is assembled by nucleons, namely protons and neutrons, has continued to attract significant attention.

Among nuclear fundamental properties, the root-mean-square (rms) proton distribution radii (R_p) and neutron distribution radii (R_n) characterize the spatial distribution sizes of protons and neutrons inside nuclei, respectively. They play an extremely important role in nuclear structure and astrophysics investigations. The global trend of nucleon radii is proportional to the cube root of mass number $A^{1/3}$, which reflects the saturation of nuclear force. Owing to the well-known electromagnetic interaction, the charge radii of approximately 1000 isotopes have already been measured with a high precision of approximately 0.01 fm [3]. With these precise radius data, for instance, the observed odd-even staggering and shape-staggering effects were applied to constrain microscopic theories [4, 5]. Combining with the proton distribution radii deduced from the measured charge radii, the neutron radii can be extracted from the measured matter (neutron+proton) radii (R_m) via $R_n = \sqrt{\frac{A}{N}R_m^2 - \frac{Z}{N}R_p^2}$, where N, Z, and A denote the neutron, proton, and mass numbers, respectively. However, the matter radius measurements are model-dependent and have relatively large uncertainties of approximately 0.05 fm due to the poorly known strong interaction [6].

Compared to the charge radii, as shown in Fig. 1, the experimental matter radius data are still scarce, and only about 200 isotopes were measured [7−11]. However, in recent decades, with the development of theories, different experimental methods, such as interaction cross sections [12], antiprotonic atoms [13], hadron scatterings [14], and parity-violation electron scatterings [15], are adopted to obtain insights into the physical quantities associated with nucleon spatial distributions in nuclei. The famous halo structure in weakly-bound nucleus ^{11}Li was found through the abnormal deviation of the measured matter radii by the interaction cross section experiments [12]. Furthermore, the neutron radii play an important role in searching new physics via atomic and particle physics experiments related to the weak interaction, *e.g.*, the atomic parity violation [16] and the coherent elastic neutrino-nucleus scattering [17]. Additionally, the difference between the neutron and proton radii in nucleus, $\Delta R_{np} = R_n - R_p$, termed as neutron skin thickness, has also been widely employed to constrain the symmetry energy

Received 6 January 2025; Accepted 12 March 2025; Published online 13 March 2025
* Supported in part by the NSFC (12375115, 12121005)
† E-mail: tuxiaolin@impcas.ac.cn
‡ E-mail: gaoqi@utibet.edu.cn

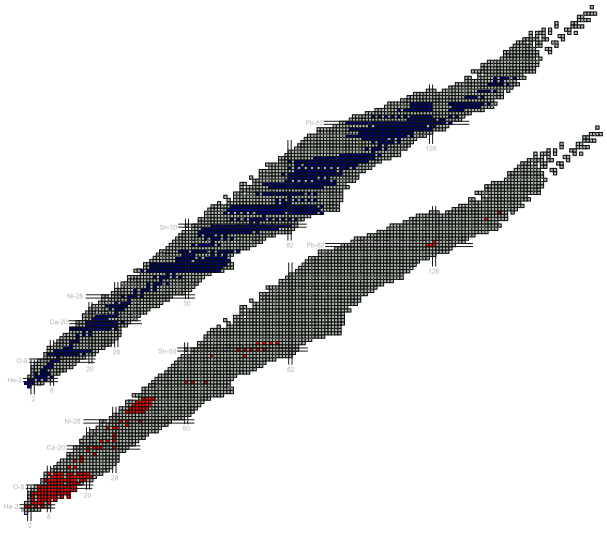

Fig. 1. (color online) Upper: Nuclides with experimental charge radius data are indicated by the filled blue squares. Lower: The filled red squares show the nuclides whose matter radii have been determined by experiments. The charge radius data can be found in Ref. [3]. Please refer to Refs. [7−11] for the matter radius data.

slope L at the saturation density [18]. Recently, the experimental neutron skin data for stable Ca, Ni, Sn, and Pb isotopes were compiled, and the evaluated neutron skin values have a precision of approximately 0.02 fm [9]. With these evaluated data, separate trends of neutron skins versus relative neutron excess, $\delta = (N-Z)/A$, were observed for Ca, Ni, Sn, and Pb isotopic chains [9]. Moreover, CREX-PREX neutron skin puzzle [19, 20], i.e., the discrepancy between the parity-violation electron scattering measurements [15, 21] with other experimental results, may also indicate new physics. Please refer to Refs. [19, 20] for more details.

It is well known that proton probe not only interacts with protons in nucleus, but also interacts with neutrons inside nucleus. With the development of ion accelerators, the wavelength of high-energy proton probe is comparable with the spatial distributions of nucleons in nucleus. Therefore, proton-nucleus elastic scattering is widely used to determine the matter radii of nuclei [14, 17, 22−29]. Specifically, when compared to other methods, proton-nucleus elastic scattering is also sensitive to the matter density distribution profile [22, 27, 28]. For example, the nucleon rearrangements for the magic number ^{56}Ni- and ^{90}Zr-cores were found recently through the matter density distribution differences obtained by the proton-nucleus elastic scattering experiments [27, 28]. Additionally, matter density profiles are sensitive to cluster structures in nuclei [30]. Considering ^{20}Ne with α+^{16}O configuration, the resulting theoretical matter density diffuseness parameter a of 0.585 fm [30] is in good agreement with a measured result of 0.592(30) fm from the proton-^{20}Ne elastic scattering experiment [31].

It should be noted that most proton-nucleus elastic scattering experiments have been performed in normal kinematics based on solid target [25, 29], which are limited to the stable or very long-lived nuclides. Furthermore, based on the thick solid-target method, it is challenging to precisely measure the low momentum transfer scattering because the ejectiles from multiple scattering would have different orbits and large energy losses. As is known, compared to inelastic scattering, the small-angle differential cross sections of proton–nucleus elastic scattering in the center-of-mass (c.m.) frame, resulting from low momentum transfer, are generally relatively high. Therefore, low momentum transfer measurements are useful in reducing the effects of inelastic scattering associated with low excitation energies. [17]. Additionally, the low momentum transfer elastic scatterings are from the peripheral collisions, and the reaction mechanism is relatively simple when compared to large-angle scatterings [29, 32]. For example, the effects of spin-orbit term can be neglected for the description of small-angle differential cross sections of proton-nucleus elastic scattering. Therefore, the matter radius extractions using the Glauber multiple-scattering model can be performed with less parameters [29, 32]. Hence, radius uncertainties caused by the input parameters would be smaller. Therefore, novel experimental methods based on active gas target and internal gas-jet target are developed to determine the matter radii by measuring the small-angle differential cross sections of proton-nucleus elastic scattering at low momentum transfer [22, 23, 32]. These types of experiments are conducted in inverse kinematics and are well-suited for studying the matter radii of gaseous and chemically active isotopes, as they circumvent the challenges associated with target production., as shown by our in-ring ^{78}Kr and ^{133}Cs experiments [17, 23].

II. IN-RING NUCLEAR REACTION FACILITY AT CSRe

The EXL cooperation group as a pioneer has already shown that various nuclear reactions induced by light ions, *e.g.*, elastic scattering [22], inelastic scattering [33], and transfer reaction [34, 35], can be effectively addressed by the in-ring experimental method based on the internal gas-jet target. The storage ring nuclear physics group at the Institute of Modern Physics (IMP) has started to develop the in-ring nuclear reaction techniques based on the Cooler Storage Ring at the Heavy Ion Research Facility in Lanzhou (HIRFL-CSR) since 2016 [36]. The HIRFL-CSR [37], as shown in Fig. 2, comprises main storage ring (CSRm) and experimental storage ring (CSRe). The two rings are connected by a radioactive beam line (RIBLL2). The primary beam with an energy of several MeV/u from the sector focusing cyclo-

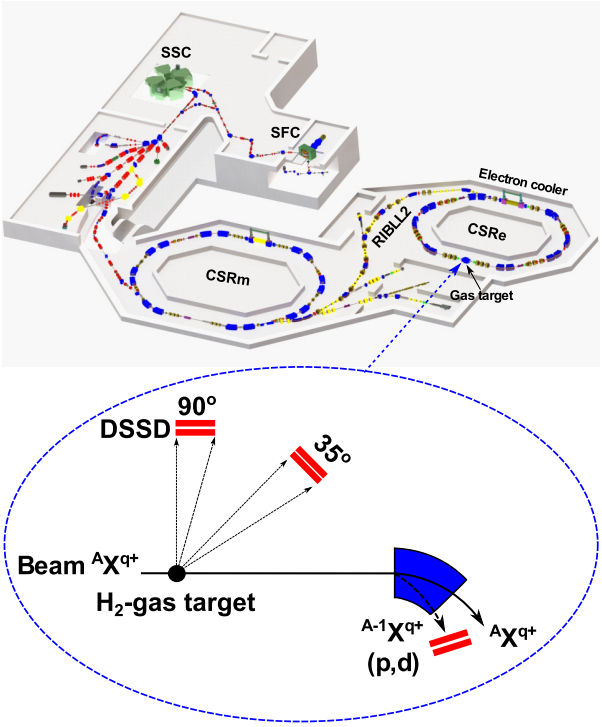

Fig. 2. (color online) Layout of HIRFL-CSR (upper) [37] and schematic illustration of the detector system installed for the in-ring nuclear reaction experiments (lower) [36].

tron (SFC) can be accelerated to an energy of several hundred MeV/u by CSRm. Secondary beam can be produced by the projectile fragmentation, and they can be subsequently purified by RIBLL2 through $B\rho$-ΔE-$B\rho$ method. The primary or secondary beam is injected and stored in CSRe for atomic and nuclear experiments. The CSRe is equipped with an electron cooler [38] and an internal gas-jet target facilities [39]. The momentum spread of stored ions can be reduced by the electron cooler [38]. Although it will take several seconds (based on numbers of ions and charge state) to reduce the momentum spread of stored ions, the in-ring nuclear reaction experiments can still cover many isotopes, as shown in Fig. 3. To produce hydrogen-gas-jet target, the hydrogen gas at a few atmospheres is cooled to a low temperature of approximatley 40 K by the internal gas-jet target. Subsequently, the cooled gas is expanded into the vacuum environment through a conical nozzle. Hence, the gas-jet beam is formed owing to the adiabatic expansion inside the nozzle. With the extraction of a set of skimmers, the produced hydrogen-gas-jet target in the collision region has a typical diameter of approximately 4 mm and thickness of approximately 10^{12} atoms/cm^2. More details on the internal gas-jet target at the CSRe can be found in Ref. [39]. The stored ions interact repeatedly with the gas-jet target based on inverse kinematics in CSRe. Various nuclear reactions, *e.g.*, elastic scattering, inelastic scattering, and transfer reaction, are induced by the collisions with

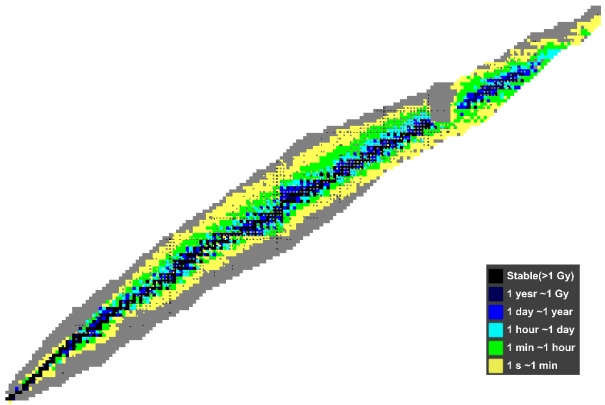

Fig. 3. (color online) Nuclei with half-lives greater than 1s in the nuclide chart, which generally can be measured by the in-ring nuclear reaction experiments. The figure is obtained by NucleusPlus software [40].

the protons in the hydrogen-gas-jet target.

For the proton-nucleus elastic scattering experiment performed in inverse kinematics (high-energy ions collide with proton target), as shown in Fig. 2, the elastic recoil protons from the low momentum transfer are measured by the Si-strip detector installed at approximately 90 degree in laboratory frame [36] to determine the small-angle differential cross sections in the center-of-mass frame. To measure the low energy protons, the Si-strip detector should be installed in the CSRe ring. Hence, the adopted Si-strip detector should satisfy the requirements of ultra-high vacuum and high temperature conditions in storage ring. Please refer to Ref. [36] for more details on the development of ultra-high vacuum compatible Si-strip detector at CSRe. The energy resolution for the used Si-strip detector after high-temperature degassing at approximately 150 °C is about 1% (FWHM), which was measured by a ^{241}Am alpha source. Additionally, the measured relative detection efficiencies are consistent in the energy range from approximately 0.5 to 5.5 MeV [23].

As shown in Fig. 3 in Ref. [39], the available flanges of the CSRe gas-target chamber at forward angle are at approximately 35 degree. Furthermore, we can mount the Si-strip detector at the flanges to measure the small-angle inelastic scattering protons in the center-of-mass frame, as shown in Fig. 2. It should be noted that to measure the small-angle inelastic scattering protons in this angular region, the beam energy should be optimized according to reaction kinematics. With the measurements of inelastic scattering proton at small angles, the isovector giant dipole resonance (IVGDR) can be examined [41]. Moreover, this detector system can be employed to measure the light recoil particles from the transfer reactions. Given the lack of decelerating facility at CSRe, the secondary beam produced by the intermediate-high energy projectile fragmentation can not be decelerated to the low energy approaching the Gamow Window. However, the

(low charged) primary beam with an energy of approximately 20 MeV/u from the CSRm can be injected and stored at CSRe. Consequently, low-energy transfer reaction experiments relevant to astrophysics can be conducted, at least for stable and long-lived isotopes. As is known, the trajectories of projectile-like products from the transfer reactions, *e.g.*, (*p*, *d*) and (*d*, *p*), can be changed in the dipole magnetic field because the mass numbers of projectile-like products differ from the stored ions. Therefore, the projectile-like products from the low energy transfer reactions can also be detected by the Si-strip detector installed behind the first dipole magnet at the CSRe, as shown in Fig. 2. To determine absolute cross sections, the reaction luminosities for the inelastic scattering and transfer reaction can be determined through comparing the measured elastic scattering differential cross sections with the calculated results based on experimentally deduced global phenomenological optical model potentials [42].

III. MATTER RADIUS MEASUREMENTS OF ^{78}Kr AND ^{133}Cs

Currently, the small-angle differential cross sections for proton-nucleus elastic scattering have been successfully measured to determine matter radii using the in-ring nuclear reaction facility at the HIRFL-CSR [17, 23, 24]. The Si-strip detector installed at approximately 90 degrees in laboratory frame is used to measure the counts and energies of the elastic recoil protons from the low momentum transfer, as shown in Fig. 2. The flight paths and energies of recoil protons are hardly altered by secondary collisions with the very thin gas-jet target. Therefore, the differential cross sections of proton-nucleus elastic scattering can be precisely obtained by the measured proton counts and energies [17, 23]. Specifically, the effects of thin target on the reaction luminosity can also be compensated by the high revolution frequencies of stored ions. Subsequently, the matter radii are extracted by fitting the measured small-angle differential cross sections with the Glauber model [43]. As is known, the slope parameters β are one of important input quantities for the Glauber model fitting [32]. To reduce the model-dependent error, the energy-dependent slope parameters were calibrated through fitting the reported small-angle differential cross sections of proton-nucleus elastic scatterings at different energies to reproduce the determined matter radii by other experiments [44]. For more details on the experiments and data analyses for the in-ring radius measurements at the HIRFL-CSR, please refer to Refs. [17, 23].

In the region of mass number around 70, the matter radii for the proton-rich Ga and Kr isotopes have been determined by the measured reaction cross sections and interaction cross sections [11, 45], respectively. Combining with proton distribution radii, the differences between neutron and proton radii can be extracted from the measured matter radii via $\Delta R_{np} = \sqrt{\frac{A}{N}R_m^2 - \frac{Z}{N}R_p^2} - R_p$. Obviously, as shown in Fig 4, negative ΔR_{np} values indicate that there are proton skin structures in this mass region. However, the proton skin structures in this mass region can result in a tension with other observables and methodologies. For example, as is known, the linear relationship between the ΔR_{np} value and the symmetry energy slope L at the saturation density can be established by the self-consistent mean-field models [46]. However, the proton skin structures with negative ΔR_{np} values in this mass region cannot be reproduced by L values in the range of 30 MeV to 110 MeV, which are constrained by different observables and methodologies [47]. To address the possible proton skin structures, a different experimental method was adopted to measure the matter radius of ^{78}Kr at HIRFL-CSR. We measured the small-angle differential cross sections of proton-^{78}Kr elastic scattering} with a collision energy of 152.7 MeV/u using the in-ring nuclear reaction facility at CSRe [23]. An rms point-matter radius of 4.16(12) fm for ^{78}Kr nucleus was obtained by fitting the measured small-angle differential cross sections with Glauber model [23]. In the fitting procedure, the relative differential cross section analysis method [10] was employed to reduce the effects of reaction luminosity on radius precision. The resulting ΔR_{np} of 0.06(22) fm for ^{78}Kr is consistent with a value of 0.03 fm predicted by the DD-ME2 interaction with a L value of 51 MeV, which is close to the world-averaged L value of 57 MeV obtained by different observables and methodologies [47]. Our results do not obviously indicate that there is a proton skin structure in ^{78}Kr.

Besides nuclear structure, ΔR_{np} data also find their

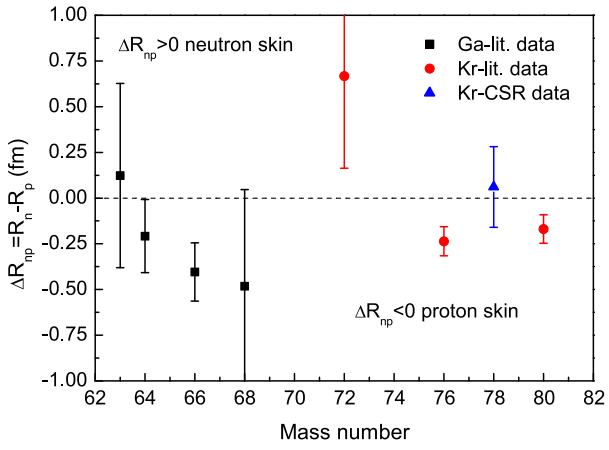

Fig. 4. (color online) Difference between neutron and proton radii, ΔR_{np}, for Ga and Kr isotopes in the region with mass number of approximately 70. The literature data for matter radii are taken from Refs. [11, 45].

applications in atomic and particle physics. The measurements of atomic parity violation for ^{133}Cs have been precisely conducted [48]. As is known, the parity violation in atom is dominated by the Z-boson exchange between atomic electrons and neutrons [49]. However, the reference many-body Coulomb-correlated amplitude for the parity-nonconserving (PNC) is usually determined using the proton distribution in nucleus [49]. Therefore, the effects of neutron-proton radius difference on the parity-nonconserving amplitude, $\frac{\delta E^{n.s.}_{\rm PNC}}{E_{\rm PNC}}$, should be considered via [49]

$$\frac{\delta E^{n.s.}_{\rm PNC}}{E_{\rm PNC}} \approx -\frac{3}{7}(\alpha Z)^2 \frac{\Delta R_{np}}{R_p}, \tag{1}$$

where α denotes the fine-structure constant.

Due to the low melting point of 28 degrees Celsius and spontaneous ignition in air, the neutron radius of ^{133}Cs is still not precisely measured. Based on the observed coherent elastic neutrino-nucleus scattering by CsI[Na] detector [50], the extracted neutron radius values for ^{133}Cs have a large spread, which depends on the adopted data analysis methods. Please refer to Ref. [17] and references cited therein for more details. Recently, the point-neutron radius of ^{133}Cs was also determined to be 4.86(21) fm by measuring proton-^{133}Cs elastic scattering at low momentum transfer at CSRe [17]. With our neutron radius, the weak mixing angle $\sin^2\theta_W$ was independently extracted as 0.227(28) by fitting the coherent elastic neutrino-nucleus scattering data [17]. Combining with the proton distribution radius, a ΔR_{np} value of 0.12(21) fm for ^{133}Cs was obtained, which is consistent with the calculated value of 0.13(4) fm by the empirical linear relationship from the antiprotonic atom experiment [13]. In the current study, we address the impact of our ΔR_{np} result for ^{133}Cs on the parity-nonconserving amplitude correction. As is known, the extracted folded-neutron radius values of ^{133}Cs from the coherent elastic neutrino-nucleus scattering experiments [50] spread from 4.6 fm through 6.6 fm [17]. These neutron radii associated with different ΔR_{np} values can result in different parity-nonconserving amplitude corrections with a standard deviation of 0.006. Please refer to the histogram in Fig. 5. With our ΔR_{np} value of ^{133}Cs, the neutron skin correction on the parity-nonconserving amplitude is determined as –0.0017(30). Obviously, the correction precision is improved by our ΔR_{np} data, as shown in Fig. 5.

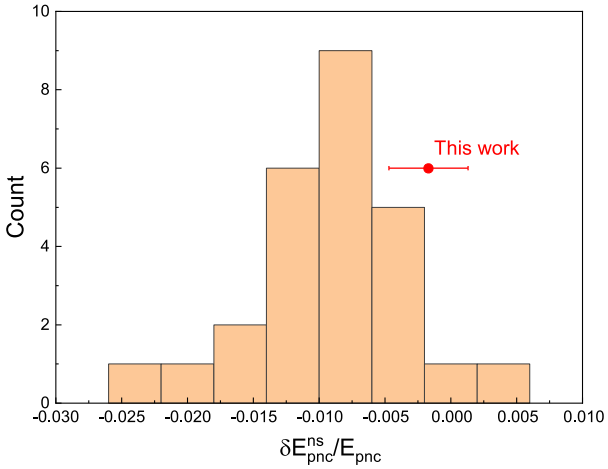

Fig. 5. (color online) Neutron skin correction for parity-nonconserving amplitude. The histogram was obtained using different neutron radii, which were extracted from coherent elastic neutrino-nucleus scattering data, details can be found in Ref. [17] and references cited therein.

IV. SUMMARY AND OUTLOOK

Direct reactions at low momentum transfer induced by light ions provide important information for examining nuclear structure and astrophysics. Recently, a novel in-ring nuclear reaction technique based on stored beam and internal gas-jet target has attracted significant interest. This method is characterized by the low-momentum sensitivity and low background. As one of the existing facilities, the HIRFL-CSR is equipped with an electron cooler and an internal gas-jet target, providing the capability to perform such experiments using inverse kinematics. In this proceeding, we present the progress of in-ring nuclear reaction studies conducted at HIRFL-CSR. Specifically, the recent matter radius determinations for ^{78}Kr and ^{133}Cs and their impacts on the skin structure and the parity-nonconserving amplitude correction were also discussed. In the near future, the one-day experiment for (p, p') inelastic scattering at the CSRe will be performed.

References

[1] H. Geiger and E. Marsden, Proc. R. Soc. Lond. A **82**, 495 (1909)
[2] E. Rutherford, Philosophical Magazine Series **21**, 669 (1911)
[3] I. Angeli and K. P. Marinova, At. Data Nucl. Data Tables **99**, 69 (2013)
[4] R. P. de Groote, J. Billowes, C. L. Binnersley *et al.*, Nat. Phys. **16**, 620 (2020)
[5] B. A. Marsh, T. Day Goodacre, S. Sels *et al.*, Nat. Phys. **14**, 1163 (2018)
[6] M. Thiel, C. Sfienti, J. Piekarewicz *et al.* , J. Phys. G: Nucl. Part. Phys. **46**, 093003 (2019)
[7] A. Ozawa, T. Suzuki, and I. Tanihata, Nucl. Phys. A **693**, 32 (2001)

[8] J. Jastrzebski, A. Trzcińska, P. Lubiński *et al.*, Int. J. Mod. Phys. E **13**, 343 (2004)
[9] J. T. Zhang, X. L. Tu, P. Sarriguren *et al.*, Phys. Rev. C **104**, 034303 (2021)
[10] Y. Huang, X. Y. Wu, X. L. Tu *et al.*, Phys. Rev. C **108**, 054610 (2023)
[11] G. F. Lima, A. Lépine-Szily, A. C. C. Villari *et al.*, Nucl. Phys. A **735**, 303 (2004)
[12] I. Tanihata, H. Hamagaki, O. Hashimoto *et al.*, Phys. Rev. Lett. **55**, 2676 (1985)
[13] A. Trzcińska, J. Jastrzebski, P. Lubiński *et al.*, Phys. Rev. Lett. **87**, 082501 (2001)
[14] G. D. Alkhazov, M. N. Andronenko, A. V. Dobrovolsky *et al.*, Phys. Rev. Lett. **78**, 2313 (1997)
[15] D. Adhikari, H. Albataineh, D. Androic *et al.*, Phys. Rev. Lett. **126**, 172502 (2021)
[16] A. Derevianko, Phys. Rev. Lett. **85**, 1618 (2000)
[17] Y. Huang, S. Y. Xia, Y. F. Li *et al.*, Phys. Lett. B **856**, 138902 (2024)
[18] B. Li, L. Chen, and C. Ko, Phys. Rep. **464**, 113 (2008)
[19] M. Atzori Corona, M. Cadeddu, N. Cargioli *et al.*, Phys. Rev. C **105**, 055503 (2022)
[20] T. G. Yue, Z. Zhang, and L. W. Chen, arXiv: 2406.03844v1
[21] D. Adhikari, H. Albataineh, D. Androic *et al.*, Phys. Rev. Lett. **129**, 042501 (2022)
[22] M. von Schmid, T. Aumann, S. Bagchi *et al.*, Eur. Phys. J. A **59**, 83 (2023)
[23] J. T. Zhang, P. Ma, Y. Huang *et al.*, Phys. Rev. C **108**, 014614 (2023)
[24] K. Yue, J. T. Zhang, X. L. Tu *et al.*, Phys. Rev. C **100**, 054609 (2019)
[25] S. Terashima, H. Sakaguchi, H. Takeda *et al.*, Phys. Rev. C **77**, 024317 (2008)
[26] G. A. Korolev, A. V. Dobrovolsky, A. G. Inglessi *et al.*, Phys. Lett. B **780**, 200 (2018)
[27] Y. Huang, L. Xayavong, X. L. Tu *et al.*, Phys. Lett. B **847**, 138293 (2023)
[28] X. Liu, P. Egelhof, O. Kiselev *et al.*, Phys. Lett. B **809**, 135776 (2020)
[29] G. D. Alkhazov, S. L. Belostotsky, and A. A. Vorobyov, Phys. Rep. **42**, 89 (1978)
[30] Y. Yamaguchi, W. Horiuchi, and N. Itagaki, Phys. Rev. C **108**, 014322 (2023)
[31] Z. H. Li, Y. Kuang, Y. Huang *et al.*, Phys. Rev. C **107**, 064310 (2023)
[32] G. D. Alkhazov, A. V. Dobrovolsky, P. Egelhof *et al.*, Nucl. Phys. A **712**, 269 (2002)
[33] J. C. Zamora, T. Aumann, S. Bagchi *et al.*, Phys. Lett. B **763**, 16 (2016)
[34] D. T. Doherty, P. J. Woods, Yu. A. Litvinov *et al.*, Phys. Scr. **T166**, 014007 (2015)
[35] J. C. Zamora, T. Aumann, S. Bagchi *et al.*, Phys. Rev. C **110**, 044614 (2024)
[36] J. T. Zhang, K. Yue, H. X. Li *et al.*, Nucl. Instrum. Methods A **948**, 162848 (2019)
[37] J. W. Xia, W. L. Zhan, B. W. Wei *et al.*, Nucl. Instrum. Methods A **488**, 11 (2002)
[38] L. J. Mao, H. Zhao, X. D. Yang *et al.*, Nucl. Instrum. Methods A **808**, 29 (2016)
[39] C. J. Shao, R. C. Lu, X. H. Cai *et al.*, Nucl. Instrum. Methods B **317**, 617 (2013)
[40] J. Y. Shi, W. J. Huang, M. Wang *et al.*, Nucl. Sci. and Tech. **35**, 186 (2024)
[41] P. von Neumann-Cosel and A. Tamii, Eur. Phys. J. A **55**, 110 (2019)
[42] J. T. Zhang, K. Yue, C. J. Shao *et al.*, Nucl. Instrum. Methods B **478**, 46 (2020)
[43] R. J. Glauber, *Lectures in Theoretical Physics*, ed. by W. E. Brittin and L. G. Dunham (Interscience, New York, 1959), Vol. 1, p. 315
[44] Y. Huang, J. T. Zhang, Y. Kuang *et al.*, Eur. Phys. J. A **59**, 4 (2023)
[45] T. Yamaguchi, T. Suzuki, T. Ohnishi *et al.*, Phys. Rev. C **77**, 034315 (2008)
[46] B. A. Brown, Phys. Rev. Lett. **85**, 5296 (2000)
[47] H. Sotani, N. Nishimura, and T. Naito, Prog. Theor. Exp. Phys. **2022**, 041D01 (2022)
[48] C. S. Wood, S. C. Bennett, D. Cho *et al.*, Science **275**, 1759 (1997)
[49] A. Derevianko, Phys. Rev. A **65**, 012106 (2001)
[50] D. Akimov, J. B. Albert, P. An *et al.*, Science **357**, 1123 (2017)